Electron-impact ionization of lithiumlike ions: Ti^{19+}, V^{20+}, Cr^{21+}, Mn^{22+}, and Fe^{23+}

K. L. Wong, P. Beiersdorfer, M. H. Chen, R. E. Marrs, K. J. Reed, J. H. Scofield, D. A. Vogel, and R. Zasadzinski

Lawrence Livermore National Laboratory, University of California, Livermore, California 94550

(Received 22 February 1993)

The Livermore electron-beam ion trap has been used to measure cross sections for electron-impact ionization of lithiumlike Ti, V, Cr, Mn, and Fe. The measurements were made using two variations of an x-ray technique that correlates ionization events with dielectronic-recombination photons. The cross sections were determined at one energy corresponding to approximately 2.3 times threshold. Ionization cross sections are measured (i) relative to the theoretical cross section for radiative recombination onto the $n=2$ shell for lithiumlike ions and (ii) relative to the theoretical cross section for direct excitation of the lithiumlike line q $[1s2s(^3S)2p\ ^2P_{3/2} \rightarrow 1s^2 2s\ ^2S_{1/2}]$. The uncertainties in the ionization cross sections are estimated to be about 10% from the experiment together with a systematic uncertainty from the choice of normalization, which is 3% for radiative recombination and 10% for direct excitation. Good agreement is found with relativistic distorted-wave calculations.

PACS number(s): 34.80.Kw, 32.70.−n, 32.30.Rj, 34.80.Dp

I. INTRODUCTION

Accurate knowledge of ionization cross sections and rates is important for determining the relative ion charge-state abundances and for interpreting the spectra observed in high-temperature laboratory and astrophysical plasmas. It is important, for example, for inferring the diffusive and convective transport of impurity ions such as titanium, chromium, and iron in tokamaks from spectral observations and for determining the power balance. High concentrations of these elements, which occur due to sputtering of wall and limiter material, are detrimental in that they cool the plasma by emitting line radiation; they can also trigger instabilities and disruptions of current flow.

Two types of measurement have provided ionization data on the transition metals. Absolute ionization cross sections of ions have been measured since 1961, when Dolder, Harrison, and Thonemann originated the crossed electron-ion beam technique [1]. Subsequently, ionization cross sections for Ti, Cr, and Fe ions with charges up to +15 have been measured using crossed beams [2–4]. Although the interaction energy was limited (≤ 1.5 keV), the results this method provides are highly accurate with typical uncertainties of 8–10%, and the cross sections are obtained as a function of electron-beam energy. Moreover, threshold processes, such as excitation-autoionization, can be studied [5].

In the second, more recent technique, ionization rates, i.e., the product of the cross section and the electron velocity averaged over the Maxwellian electron velocity distribution, have been measured using plasma spectroscopy. This technique involves modeling the time evolution of x-ray line emission following the initial compression in θ pinches [6] or after the sawtooth instability in tokamaks [7]. Due to low electron temperatures, θ pinches are limited to measuring ionization rates for low charge states, e.g., Ti^{8+} [8]. High-temperature devices such as tokamaks have been used to infer ionization rates in Ti and Fe for charge states up to +21 [9,10]. However, a sensitivity study shows the rates accurate to only 20–40% [9,10].

This paper describes ionization measurements of highly charged lithiumlike titanium ($Z=22$), vanadium ($Z=23$), chromium ($Z=24$), manganese ($Z=25$), and iron ($Z=26$) ions made on an electron-beam ion trap (EBIT) using a technique that relies on x-ray observations. EBIT is a tool for studying highly charged ions, presently up to U^{89+} [11–13]. The technique we describe thus allows us in principle to measure the ionization cross section of any lithiumlike ion, and a measurement of the ionization cross section of lithiumlike Ba^{53+} was reported earlier [14]. These charge states are much higher than those available with either the crossed-beam or the plasma-spectroscopy approaches. Moreover, EBIT has the advantage of measuring electron-ion collision cross sections rather than rates and thus testing theory in a more direct way. In the current set of ionization measurements the electron-beam energy is a factor of two to three times higher than the beam energy of the crossed-beam experiments, and the uncertainties in our technique are generally lower than those of the plasma-spectroscopy measurements.

II. DESCRIPTION OF TECHNIQUE

The measurement scheme is based on a steady-state balance between the processes of dielectronic recombination and ionization. The scheme is illustrated in Fig. 1. In the scheme shown we have neglected radiative and charge-exchange recombination onto heliumlike ions, which we later show to be small, although we make corrections for them in the final analysis. With the electron-beam energy set to the *KLL* dielectronic resonance energy for heliumlike ions, the abundance ratio of the heliumlike and lithiumlike charge states is equal to the ratio of the cross sections for ionization and dielect-

 ©1993 The American Physical Society

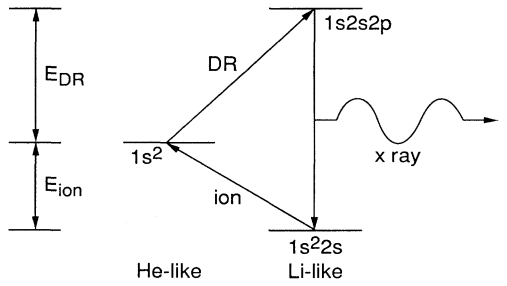

FIG. 1. Steady-state measurement scheme for lithiumlike ions. By counting the $n=2\rightarrow 1$ x rays given off in the dielectronic recombination of heliumlike ions the ionization cross section can be measured. E_{DR} and E_{ion} represent the dielectronic-recombination energy for heliumlike ions and ionization energy of lithiumlike ions. The arrows labeled DR, x ray, and ion represent the dielectronic recombination of heliumlike ions, the x rays emitted, and the ionization of lithiumlike ions, respectively.

ronic recombination. As a result, an x ray emitted during dielectronic recombination indicates that an ionization event has occurred, and we determine the ionization cross section by counting the $n=2\rightarrow 1$ dielectronic-recombination x rays.

A different but related scheme was used recently to measure the dielectronic-recombination cross sections of Ar^{16+} on an electron-beam ion source (EBIS) [15,16]. Ali and co-workers measured dielectronic recombination by extracting the ions, counting the electron energy-dependent yields of heliumlike and lithiumlike argon ions, and normalizing to the theoretical ionizations cross section of lithiumlike argon. On the other hand, we measure ionization by counting dielectronic-recombinations x rays and normalizing to either theoretical radiative-recombination or excitation cross sections without requiring detailed knowledge of the dielectronic process itself.

The general rate equation for the density of heliumlike ions, which includes the processes of radiative recombination and charge-exchange recombination with residual gas atoms in EBIT, is given by

$$\frac{dn_{\mathrm{He}}}{dt}=\frac{j_e}{e}(\sigma_i n_{\mathrm{Li}}-\sigma_{\mathrm{DR}}n_{\mathrm{He}}-\sigma_{\mathrm{RR}}n_{\mathrm{He}})-n_0 v_0\sigma_{\mathrm{cx}}n_{\mathrm{He}}\ , \tag{1}$$

where j_e is the effective current density, e is the charge of the electron, σ_i is the cross section for ionization of a lithiumlike ion, σ_{DR} and σ_{RR} the cross sections for dielectronic and radiative recombination onto the heliumlike ion, and σ_{cx} the cross section for charge-exchange recombination with neutral background gases. The number densities of ground-state heliumlike and lithiumlike ions are n_{He} and n_{Li}, n_0 is the density of neutral background atoms, and v_0 is the relative velocity of the neutrals and ions. The density of hydrogenlike ions plays no role in Eq. (1) because the electron-beam energies in the measurements are always below the ionization threshold energy to produce hydrogenlike ions. In steady state, $dn_{\mathrm{He}}/dt=0$, so we can express σ_i as

$$\sigma_i=\frac{n_{\mathrm{He}}}{n_{\mathrm{Li}}}\left[\sigma_{\mathrm{DR}}+\sigma_{\mathrm{RR}}+\frac{en_0v_0}{j_e}\sigma_{\mathrm{cx}}\right]\ . \tag{2}$$

In the next two subsections we discuss how we determine the quantities on the right-hand side of Eq. (2) and thus the ionization cross section from x-ray measurements involving a Ge detector and a crystal spectrometer.

A. Ge-detector measurements

In the first approach we determine the ionization cross section from x-ray observations using the solid-state Ge detector supplemented by measurements with the crystal spectrometer. With the Ge detector we observe the intensities of the x rays produced by dielectronic recombination onto heliumlike ions and by radiative recombination onto the $n=2$ shell of lithiumlike ions, respectively. They are expressed as

$$I_{\mathrm{DR}}^{\mathrm{Ge}}=\frac{j_e}{e}\sigma_{\mathrm{DR}}n_{\mathrm{He}}A_1G_1\ , \tag{3}$$

$$I_{\mathrm{RR}}^{\mathrm{Li}}=\frac{j_e}{e}\sigma_{\mathrm{RR}}^{\mathrm{Li}}n_{\mathrm{Li}}G_1\ , \tag{4}$$

where $\sigma_{\mathrm{RR}}^{\mathrm{Li}}$ is the radiative-recombination cross section onto lithiumlike ions at 90° (the angular distribution has been folded in), and A_1 represents the angular distribution factor of the dielectronic-recombination x rays. G_1 is the solid angle subtended by the Ge detector. Substituting these into Eq. (2) for n_{He} and n_{Li} we get

$$\sigma_i=\frac{I_{\mathrm{DR}}^{\mathrm{Ge}}}{I_{\mathrm{RR}}^{\mathrm{Li}}}\frac{\sigma_{\mathrm{RR}}^{\mathrm{Li}}}{A_1}\left[1+\frac{\sigma_{\mathrm{RR}}}{\sigma_{\mathrm{DR}}}+\frac{en_0v_0}{j_e}\frac{\sigma_{\mathrm{cx}}}{\sigma_{\mathrm{DR}}}\right]\ . \tag{5}$$

Because of the limited resolution of the Ge detector, the x rays from radiative recombination onto the $n=2$ shell of heliumlike, lithiumlike, and berylliumlike ions are unresolved, and we must determine the fraction that is due to recombination onto lithiumlike ions. $I_{\mathrm{RR}}^{\mathrm{Li}}$ can be expressed as

$$I_{\mathrm{RR}}^{\mathrm{Li}}=I_{\mathrm{RR}}^{\mathrm{tot}}\left[\frac{n_{\mathrm{Li}}\sigma_{\mathrm{RR}}^{\mathrm{Li}}}{n_{\mathrm{He}}\sigma_{\mathrm{RR}}^{\mathrm{He}}+n_{\mathrm{Li}}\sigma_{\mathrm{RR}}^{\mathrm{Li}}+n_{\mathrm{Be}}\sigma_{\mathrm{RR}}^{\mathrm{Be}}}\right]\ , \tag{6}$$

where $I_{\mathrm{RR}}^{\mathrm{tot}}$ is the total number of radiative-recombination photons onto the $n=2$ shell at 90°, and $\sigma_{\mathrm{RR}}^{\mathrm{He}}$ and $\sigma_{\mathrm{RR}}^{\mathrm{Be}}$ are the radiative-recombination cross sections at 90° onto the heliumlike and berylliumlike charge states, respectively. The term in parentheses on the right side of Eq. (6) represents the fraction of the radiative-recombination x rays due to the lithiumlike charge state. Substituting Eq. (6) into Eq. (5) we get

$$\sigma_i=\frac{I_{\mathrm{DR}}^{\mathrm{Ge}}}{I_{\mathrm{RR}}^{\mathrm{tot}}}\left[1+\frac{\sigma_{\mathrm{RR}}^{\mathrm{He}}n_{\mathrm{He}}}{\sigma_{\mathrm{RR}}^{\mathrm{Li}}n_{Li}}+\frac{\sigma_{\mathrm{RR}}^{\mathrm{Be}}n_{\mathrm{Be}}}{\sigma_{\mathrm{RR}}^{\mathrm{Li}}n_{\mathrm{Li}}}\right]\times\frac{\sigma_{\mathrm{RR}}^{\mathrm{Li}}}{A_1}\left[1+\frac{\sigma_{\mathrm{RR}}}{\sigma_{\mathrm{DR}}}+\frac{en_0v_0}{j_e}\frac{\sigma_{\mathrm{cx}}}{\sigma_{\mathrm{DR}}}\right]\ . \tag{7}$$

The ionization cross section thus can be evaluated from

the measured values of I_{DR}^{Ge} and I_{RR}^{tot} and normalizing to the radiative-recombination cross section σ_{RR}^{Li}. Unfortunately, there is no reliable way to determine the relative charge-state abundances n_{He}/n_{Li} an n_{Be}/n_{Li} from Ge-detector measurements. Instead, they are determined from measurements of the direct excitation line rations I_w/I_q and I_β/I_q, respectively, which were monitored with the crystal spectrometer at the same time the radiative-recombination photons onto the $n=2$ shell were being acquired with the Ge detector. Determination of charge-state ratios from crystal-spectrometer measurements is discussed in detail in Ref. [17], and the formula for I_q, etc. used to extract the charge fraction from the crystal measurements is given in the next section. Since the dielectronic-recombination rate is very large if the beam energy is set to the resonance energy, the second to the last (radiative recombination) and the last (charge-exchange recombination) term in Eq. (7) are $\ll 1$. For example, for iron at 4.64 keV the theoretical ratio of the radiative-recombination [18] and the dielectronic-recombination [19] cross sections is 0.012, and the charge-exchange term inferred from the comparison of steady-state data with the model spectra discussed later is 0.016. The ionization cross-section measurement is thus insensitive to corrections used to account for these terms. For normalization we use radiative-recombination cross sections calculated with the methods in Ref. [18]. The radiative-recombination code has been compared to measurements of photoionization, the inverse process of radiative recombination, at photon energies similar to the present experiments. The agreement is within a few percent [20].

We need to take into account the angular distribution of the dielectronic-recombination x rays as well as unresolved contributions to I_{DR}^{Ge} from satellite lines produced in the dielectronic recombination of lithiumlike ions. Since the energy of ionization measurements is always close to the energy of the heliumlike dielectronic satellites j and k, we set $A_1=1.22$, which is the average of the angular distribution correction for these satellites [21]. For the runs in which the dielectronic recombination of lithiumlike ions occurs, I_{DR}^{Ge} is multiplied by the fraction of the heliumlike dielectronic-recombination x rays relative to the total as measured by the crystal spectrometer. This fraction is never smaller than 74%.

The measurements of I_{DR}^{Ge} and I_{RR}^{tot} are also affected by absorption of the x rays by the beryllium window on the detector and on EBIT and also by the small air gap between EBIT and the solid-state detector, and we correct for these. These absorb the lower-energy dielectronic x rays more than the higher-energy radiative-recombination x rays, and thus lead to a differential change in the detection efficiency. The largest change occurred for the Ti data, where the dielectronic-recombination x rays were attenuated by 23% more than the radiative-recombination x rays.

B. High-resolution crystal-spectrometer technique

In this measurement scheme we determine lithiumlike ionization cross sections solely with a crystal spectrometer by counting the dielectronic-recombination x rays and normalizing to the theoretically calculated excitation cross section of the lithiumlike line q $[1s2s(^3S)2p\ ^2P_{3/2}\rightarrow 1s^2 2s\ ^2S_{1/2}]$.

The x-ray intensities of dielectronic recombination onto heliumlike ions and of the direct excitation of the lithiumlike line q as measured by a Bragg crystal spectrometer at 90° to the electron beam are expressed as

$$I_{DR}=\frac{j_e}{e}\sigma_{DR}n_{He}W_{DR}G_2\ , \tag{8}$$

$$I_q=\frac{j_e}{e}\beta_r\sigma_q n_{Li}W_q G_2\ , \tag{9}$$

where σ_q is the excitation cross section of the lithiumlike line q, and β_r is the radiative branching ratio of line q. G_2 is the solid angle subtended by the spectrometer. W accounts for the angular distribution of the x rays, the linear polarization of the x rays, and the reflectivity of the analyzing crystal. We use the theoretical values for polarization of the dielectronic-recombination x rays calculated by Inal and Dubau [21].

Substituting Eq. (8) and Eq. (9) into Eq. (2) for n_{He} and n_{Li}, we get

$$\sigma_i=\frac{I_{DR}}{I_q}\frac{\beta_r\sigma_q W_q}{W_{DR}}\left[1+\frac{\sigma_{RR}}{\sigma_{DR}}+\frac{en_0v_0}{j_e}\frac{\sigma_{cx}}{\sigma_{DR}}\right]\ . \tag{10}$$

The ionization cross section in Eq. (10) is evaluated using the measured values of I_{DR} and I_q. The radiative branching ratios are calculated using the methods of Ref. [22]. We normalize the measurement to theoretical excitation cross sections of line q determined from the distorted-wave code of Zhang, Sampson, and Clark [23]. We made some experimental measurements of line q in Ref. [24] and noted good agreement with distorted-wave calculations. As discussed in the preceding section, the radiative and charge-exchange terms represent only small corrections.

III. EXPERIMENTAL ARRANGEMENT

EBIT uses an electron beam to produce, trap, and excite highly charged ions [11]. Low-charged ions enter the trap from a metal vapor vacuum arc (MEVVA) ion source [25] and are trapped axially by the two end drift tubes which are biased positive with respect to the center drift tube. The electron beam ≤ 240 mA, compressed to a radius of roughly 35-μm by a 3-T magnet, traps the ions radially and successively ionizes the ions to the desired charge state. The x rays are viewed through ports at 90° to the electron beam.

The x rays are monitored with a solid-state Ge detector and a curved-crystal Bragg spectrometer in the von Hámos geometry [26]. The crystal spectrometer employs a LiF(200) crystal with a lattice spacing of $2d=4.027$ Å. The crystal was bent to a radius of curvature of 30 cm for chromium, manganese, and iron and 75 cm for titanium and vanadium. The resolving power of the setup is $\lambda/\Delta\lambda\approx 1500$ for the 30-cm crystal and $\lambda/\Delta\approx 4000$ for the 75-cm crystal. For the case of iron which we will discuss in this article, the spectrometer was set to a nominal

Bragg angle of 26.8°, which corresponds to a wavelength of 1.81 Å. The total wavelength covered was 1.77 Å $< \lambda <$ 1.88 Å which includes the heliumlike transitions w ($1s2p\ ^1P_1 \rightarrow 1s^2\ ^1S_0$) at 1.8505 Å, x ($1s2p\ ^3P_2 \rightarrow 1s^2\ ^1S_0$) at 1.8555 Å, y ($1s2p\ ^3P_1 \rightarrow 1s^2\ ^1S_0$) at 1.8595 Å, and z ($1s2s\ ^3S_1 \rightarrow 1s^2\ ^1S_0$) at 1.8682 Å [27], as well as the lithiumlike satellite lines.

A typical x-ray spectrum taken with the electron-beam energy set to the iron *KLL* dielectronic resonance is given in Fig. 2(a) for the Ge detector. Figure 2(b) shows the corresponding spectrum recorded with the crystal spectrometer. The spectrum shows the lithium dielectronic-recombination satellite lines e ($1s2p^2\ ^4P_{5/2} \rightarrow 1s^22p\ ^2P_{3/2}$), j ($1s2p^2\ ^2D_{5/2} \rightarrow 1s^22p\ ^2P_{3/2}$), k ($1s2p^2\ ^2D_{3/2} \rightarrow 1s^22p\ ^2P_{1/2}$), and a blend of s [$1s2s(^1S)2p\ ^2P_{3/2} \rightarrow 1s^22s\ ^2S_{1/2}$] and t [$1s2s(^1S)2p\ ^2P_{1/2} \rightarrow 1s^22s\ ^2S_{1/2}$]. These spectra are used to provide a count of the number of ionization events from the dielectronic-recombination x rays. An x-ray spectrum which is acquired when the electron-beam energy is changed for 6 ms away from the *KLL* resonance and set to a value where direct excitation is the only excitation mechanism is shown in Fig. 3(a) for the Ge detector. We observe both the $n=2 \rightarrow 1$ x rays and x rays

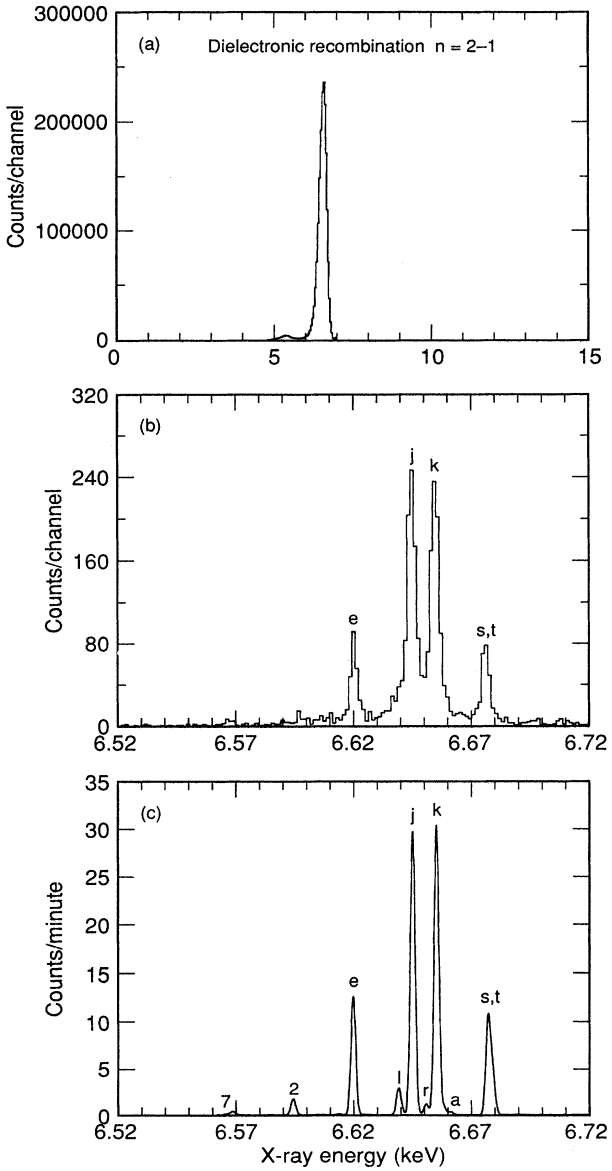

FIG. 2. Dielectronic-recombination x-ray spectrum of iron at an electron-beam energy of 4.64 keV (a) measured with a solid-state Ge detector, (b) measured with a Bragg crystal spectrometer, and (c) modeled with an electron-beam width of 40 eV (FWHM). The marked lines are identified in the text.

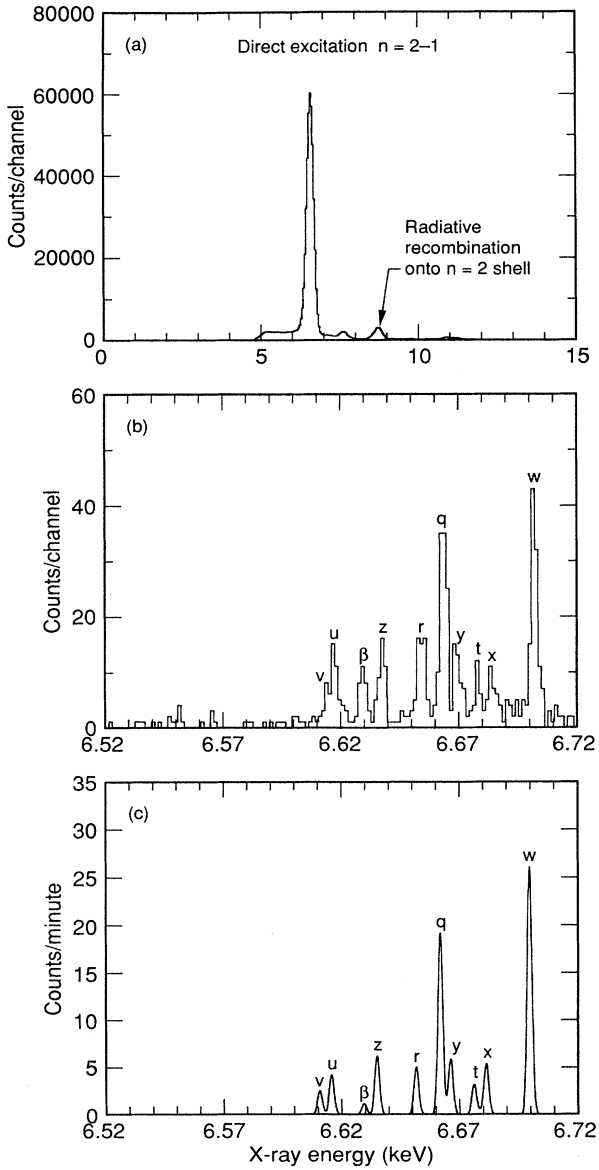

FIG. 3. Direct excitation x-ray spectrum of iron at an electron-beam energy of 6.8 keV (a) measured with a solid-state Ge detector, (b) measured with a Bragg crystal spectrometer, and (c) modeled with an electron-beam width of 40 eV (FWHM). The marked lines are identified in the text.

from radiative recombination onto the $n=2$ shell. Figure 3(b) shows the corresponding spectrum recorded with the crystal spectrometer. The heliumlike transitions w, x, y, and z, the lithiumlike transitions t, q, r [$1s2s(^3S)2p\ ^2P_{1/2} \rightarrow 1s^2 2s\ ^2S_{1/2}$], u ($1s2s2p\ ^4P_{3/2} \rightarrow 1s^2 2s\ ^2S_{1/2}$), and v ($1s2s2p\ ^4P_{1/2} \rightarrow 1s^2 2s\ ^2S_{1/2}$), and the berylliumlike transition β ($1s2s^2 2p\ ^1P_1 \rightarrow 1s^2 2s^2\ ^1S_0$) are identified in the figure. The purpose of these spectra is to provide information on the relative charge-state abundances from the radiative recombination onto the $n=2$ shell and the direct excitation x rays.

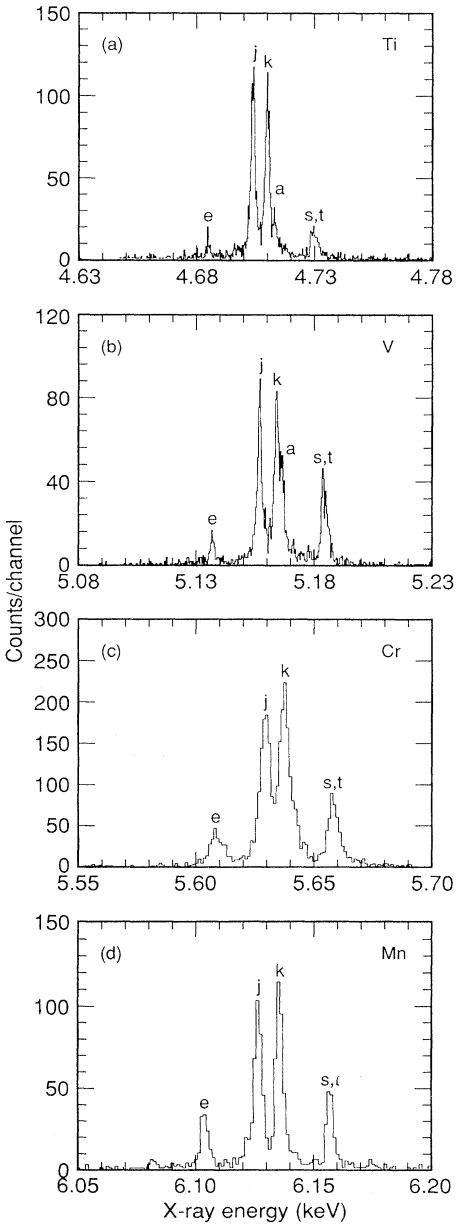

FIG. 4. Dielectronic-recombination x-ray spectrum of (a) titanium at 3.31 keV, (b) vanadium at 3.61 keV, (c) chromium at 3.95 keV, and (d) manganese at 4.28 keV. The marked lines are identified in the text.

Figures 2(c) and 3(c) give the results of an x-ray model, which we describe later.

The ionization experiment was performed by alternating the electron-beam energy between two values and recording separate spectra with the Ge detector and the crystal spectrometer. Initially, the electron-beam energy was set to the *KLL* resonance, situated at electron energies between 4.54 and 4.76 keV, for a period of 24 ms; this establishes the steady-state condition. We then probe the charge-state balance for 6 ms at 6.8 keV, which is above the direct excitation threshold for the $n=2 \rightarrow 1$ x-ray transitions and away from any resonances in order to measure lines w, q, and β. The data are divided into 15 2-ms bins. The dielectronic-recombination x rays are summed from the last 4 ms of the 24 ms on the *KLL* resonance as shown in Figs. 2(a) and 2(b). The first 20 ms on this portion of the cycle allows the charge states to reach steady state. The direct excitation spectrum is acquired during the last 4 ms of the 6 ms at 6.8 keV as shown in Figs. 3(a) and 3(b). We omit the first 2-ms time group, acquired while the beam energy is changed to the direct excitation energy, in order to allow the drift tube voltage to reach a steady value of 6.8 keV.

We made ionization measurements on the KLL resonance of iron at different beam energies ranging from 4.62 to 4.68 keV, titanium from 3.31 to 3.35 keV, vanadium from 3.61 to 3.66 keV, chromium from 3.95 to 4.00 keV, and manganese from 4.28 to 4.35 keV in 10-eV steps. Examples of the dielectronic-recombination spectra for Ti, V, Cr, and Mn are shown in Figs. 4(a)–4(d).

IV. ANALYSIS

Our measurement scheme provides the most accurate results for electron-beam energies near the dielectronic resonance energy of satellites j and k, where the dielectronic resonance strength is largest. For energies below this range, dielectronic recombination is weak, and radiative and charge-exchange recombination have large relative contributions. For energies above this range, beam electrons sample dielectronic resonances in lithiumlike ions, and transitions in berylliumlike ions begin to appear in the spectrum; at the same time the heliumlike dielectronic satellites become weaker, and, again, the scheme provides less accurate results because dielectronic recombination is weaker relative to radiative and charge-exchange recombination. For example, charge-exchange recombination is difficult to account for because we do not know the exact background neutral gas density in EBIT, and its contribution must be estimated. In addition, if radiative recombination is large this introduces an unresolved background in $I_{\mathrm{DR}}^{\mathrm{Ge}}$ [14], which must be subtracted. By setting the beam energy to the resonance energy of j and k we avoid such complications and can treat these processes as perturbations, whose contributions are small.

We determined from a model of the ionization balance in EBIT that the lithiumlike iron charge state established during the 24-ms dielectronic-recombination phase of the measurement cycle was significantly reionized during the 6-ms probing time at 6.8 keV. This causes the steady-

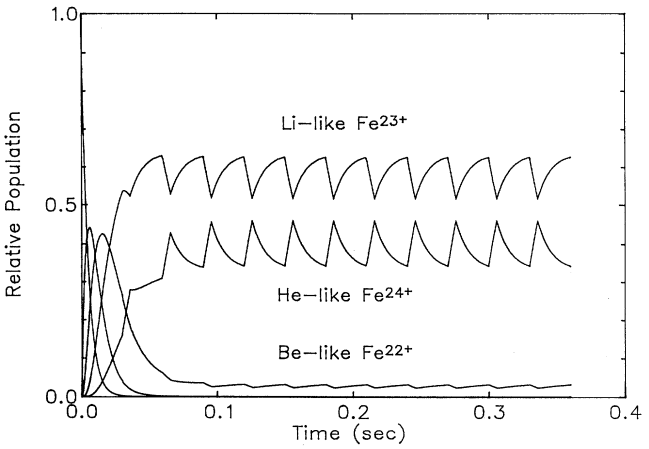

FIG. 5. The computed relative charge-state balance of iron as a function of time. The computer model includes contributions from dielectronic recombination, ionization, radiative recombination, and charge-exchange recombination. The cycle remains at 4.64 keV for 24 ms, switching to 6.8 keV for 6 ms.

state lithiumlike ion density, inferred from the direct excitation measurement of line q at 6.8 keV, to be underestimated. The modeled charge-state abundances are shown in Fig. 5 for a cycle of 24 ms at the dielectronic energy of 4.64 keV, which is a value close to the resonance energy of satellites j and k, and 6 ms at the direct excitation beam energy of 6.8 keV. The model assumes an electron beam with full width at half maximum (FWHM) of 40 eV and uses heliumlike and lithiumlike dielectronic-recombination cross sections calculated by the method of Chen [19], the Lotz formula [28] is used for ionization, and scaling formulas by Kim and Pratt [29] and by Janev, Belić, and Bransden [30] are used for radiative recombination and charge-exchange recombination, respectively. The time it takes the ion density to fall to $1/e$ of its original value at an electron-beam energy of 4.64 keV and a beam current of 148 mA are 5.4 ms for dielectronic recombination onto heliumlike iron, 8 ms for ionization of lithiumlike iron, 465 ms for radiative recombination onto the heliumlike state, and 338 ms for charge-exchange recombination between heliumlike iron and the surrounding background gas assumed to be hydrogen at a density of 1.1×10^{7} cm^{-3}.

Because significant reionization takes place during the 6 ms at 6.8 keV, the lithiumlike abundance is reduced compared to the amount present at the end of the dielectronic-recombination part of the measurement cycle. To a first approximation this can be accounted for by a correction factor determined by our model. Specifically, for the Ge-detector measurements I_{RR}^{tot} is adjusted by a factor which uses the computed relative change in the lithiumlike ion density between the last 4 ms of the 24 ms on the KLL resonance and the last 4 ms of the 6 ms on the direct excitation portion of the cycle. Similarly, for the high-resolution measurements the direct excitation measurement of the lithiumlike line q is multiplied by a factor that uses the computed average ratio of the integrated lithiumlike abundance for the last 4 ms of the 24 ms on the KLL resonance and the last 4 ms of the 6 ms on the direct excitation portion of the cycle. Table I gives the correction factors for the solid-state (Ge) detector measurements and for the von Hámos (vH) crystal-spectrometer measurements for iron at beam energies of 4.62–4.68 keV assuming the surrounding background gas to be hydrogen at a density of 1.1×10^{7} cm^{-3}. We explain how we determine this density below.

We deem the model calculation of the relative change in the ion abundances accurate to within 25%. Since they affect the determination of the ionization cross section by less than 20%, the uncertainty introduced by this procedure is no more than 5%. This is born out by a study of how the correction factors varied as the input model parameters were varied. For examples, a background gas density five times larger and five time smaller translates into a 3% change in the correction factors. Similarly, a change in the electron-beam width from 40 to 60 eV results in a 3.6% change in the correction factors.

The charge-state abundances of heliumlike, lithiumlike, and berylliumlike iron from our ionization balance model were then combined with calculated x-ray energies and cross sections of dielectronic recombination [19,22] and of direct excitation [23] to generate synthetic x-ray spectra which could be compared directly with the measured spectra. The predicted iron x-ray spectrum for dielectronic recombination corresponding to the experimental conditions in Fig. 2(b) is shown in Fig. 2(c). The peak labeled s,t contains 33% of satellite s and 67% of

TABLE I. Fe correction factors for the ionization measurements using the solid-state (Ge) detector measurements and for the von Hámos (vH) crystal-spectrometer measurements at electron-beam energies (E_{beam}) of 4.62–4.68 keV. We assume the surrounding background gas to be hydrogen at a density of 1.1×10^{7} cm^{-3}.

E_{beam} (keV)	Ge $\dfrac{I_{RR}^{Li}(\text{no reionization})}{I_{RR}^{Li}(\text{actual reionization})}$	vH $\dfrac{I_q(\text{no reionization})}{I_q(\text{actual reionization})}$
4.62	1.150	1.128
4.63	1.163	1.131
4.64	1.173	1.132
4.65	1.180	1.133
4.66	1.183	1.131
4.67	1.178	1.127
4.68	1.154	1.107

satellite t. The model spectrum also shows the lithiumlike satellites l $(1s2p^2\,{}^2D_{3/2}\rightarrow 1s^2 2p\,{}^3P_{3/2})$, r $(1s2s2p\,{}^2P_{1/2}\rightarrow 1s^2 2s\,{}^2S_{1/2})$, and a $(1s2p^2\,{}^2P_{3/2}\rightarrow 1s^2 2p\,{}^2P_{3/2})$, which are unresolved by the spectrometer. The small peaks labeled 7 and 2 are the contributions from the berylliumlike satellites $(1s2s2p_{1/2}2p_{3/2})_3\rightarrow(1s^2 2s 2p_{3/2})_2$ and $(1s2s^2 2p_{1/2})_1\rightarrow(1s^2 2s^2)_0$, respectively. A synthetic iron spectrum corresponding to direct excitation at 6.8 keV is show in Fig. 3(c). A comparison between the synthetic and experimental spectra shows good agreement and validates our model calculations. This agreement is obtained with only one free parameter in the x-ray model, namely, the charge-exchange contribution, as discussed below.

With our x-ray model we can also estimate the effect of charge-exchange recombination. During an experiment we record an x-ray spectrum at a single beam energy, i.e., without switching, as shown in Figs. 6(a) and 6(b) for iron at 6.8 keV. In steady state at this beam energy, ionization of the lithiumlike state is balanced by radiative recombinations and charge-exchange recombinations onto the heliumlike state, as shown in Eq. (1) without the dielectronic-recombination term. Since ionization and radiative recombination are known from calculations in the x-ray model, the only unknown is the charge-exchange recombination term. Consequently, the hydrogen (or equivalent) neutral density in the x-ray model is adjusted until the predicted heliumlike to lithiumlike ratio matches the measured ratio. The result of the calculation is used to account for the charge-exchange recombination term in Eqs. (7) and (10). The result of the modeled direct excitation x-ray spectrum is shown in Fig. 6(c). The neutral density that provides a match to the observed ionization balance is 1.1×10^7 cm^{-3} of H_2. The charge-exchange term we infer from the x-ray model is 1.33 times larger than the radiative-recombination term. As mentioned above, both modes of recombination are small compared to dielectronic recombination, and the ionization cross sections we measure are very insensitive to changes in the assumed background neutral density.

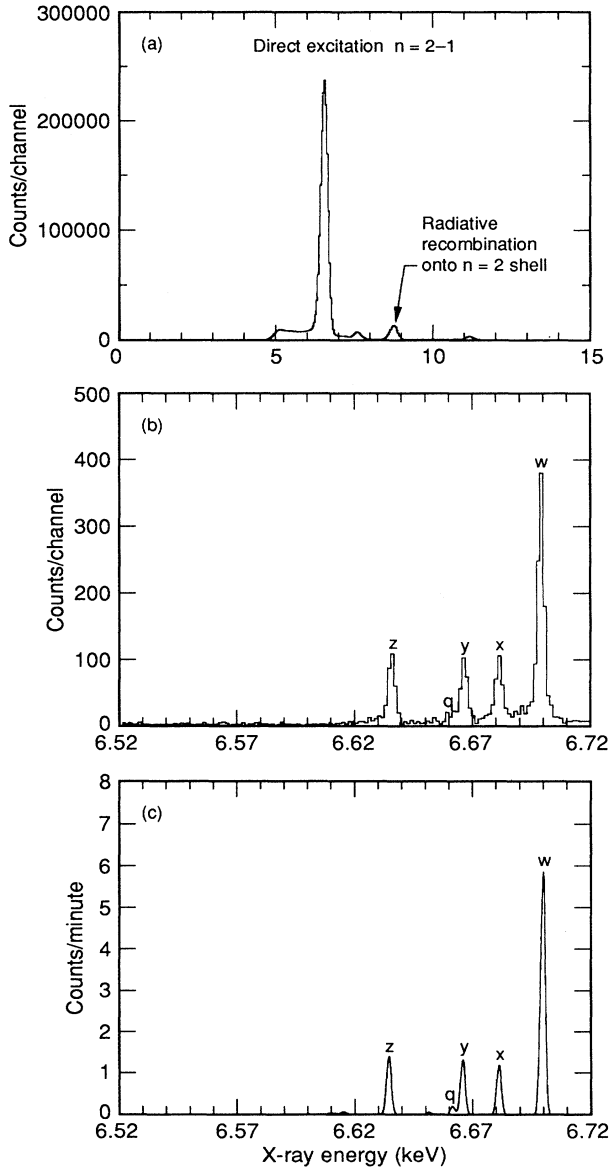

FIG. 6. Steady-state direct excitation x-ray spectrum of iron at an electron-beam energy of 6.8 keV (a) measured with a solid-state Ge detector, (b) measured with a Bragg crystal spectrometer, and (c) modeled with an electron-beam width of 40 eV (FWHM).

V. RESULTS

The results for ionization of lithiumlike ions averaged over the electron energies near the dielectronic resonance energy of satellites j and k are given in Table II. The vanadium measurements from the Ge-detector data were

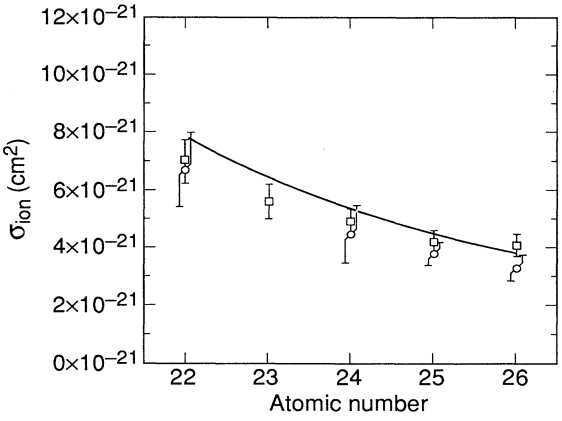

FIG. 7. Measurement of the electron-impact ionization cross section of lithiumlike ions using the solid-state Ge detector (circles) and the crystal spectrometer (squares) vs atomic number. The measurements were made at an energy corresponding to 2.3 times the threshold energy for ionization of lithium ions. The solid curve represents results from the relativistic distorted-wave calculation. Only experimental uncertainties are shown. Additional uncertainties of 3% and 10% arise from the normalization to the theoretical radiative-recombination cross section and to the theoretical direct excitation cross section of line q for the Ge-detector and crystal-spectrometer results, respectively.

TABLE II. Electron-impact ionization cross sections of lithiumlike ions in units of 10^{-21} cm^2. The energy listed is an average of several measurements close to the dielectronic resonance energy of satellites j and k. Ge represents the measurements made with the solid-state detector. vH represents the measurements made using the high-resolution spectrometer that are normalized to the theoretical [23] values of the excitation cross section of line q. Average represents the weighted average of the Ge and vH results. DW and Lotz are the distorted-wave and Lotz formula results, respectively.

		Cross Section				
Element	Energy (keV)	Ge	vH	Average	DW	Lotz
Ti^{9+}	3.33	6.67±1.33	6.98±0.75	6.91±0.65	7.81	8.04
V^{20+}	3.64		5.58±0.58	5.58±0.58	6.40	6.62
Cr^{21+}	3.97	4.44±1.02	4.88±0.44	4.81±0.40	5.35	5.50
Mn^{22+}	4.31	3.70±0.41	4.22±0.37	3.99±0.28	4.44	4.61
Fe^{23+}	4.66	3.27±0.42	4.09±0.38	3.72±0.28	3.80	3.89

omitted because an unknown impurity was present in the trap during these measurements that precluded a determination of the ionization cross section because it emitted radiation that partially overlapped with the vanadium I_{RR}^{tot}. However, we were able to infer an ionization cross section from the vanadium high-resolution data that was normalized to the theoretical cross section of line q. We also give a weighted average of the results from both methods. The results are graphically displayed in Fig. 7.

We estimate a typical experimental uncertainty of about 10% for our individual measurements. The individual sources of uncertainty are listed in Table III for the solid-state Ge-detector measurements and Table IV for the high-resolution von Hámos spectrometer measurements. We calculated the total uncertainty from the quadrature sum of all the individual sources. There is an additional systematic uncertainty from the normalization to the theoretical radiative-recombination cross sections (3%) and the direct excitation cross section of line q (10%). The largest source of uncertainty in the solid-state detector measurements is in the determination of the fraction of the total $n=2$ radiative-recombination photons from lithiumlike ions, which was determined from the crystal-spectrometer line ratio measurements. Another large source of uncertainty arises from the possibility of x radiation from background ions overlapping the radiative-recombination photons I_{RR}^{tot}, as was the case for Ti and Cr. The largest uncertainties in the high-resolution von Hámos spectrometer measurements are in the theoretical radiative branching ratios and the response linearity of the crystal used in the Bragg spectrometer.

The results of our measurements are compared to theoretical values calculated using the relativistic distorted-wave code of Zhang and Sampson [31] and to the semiempirical Lotz formula [28]. Almost all measured cross sections are lower than calculated, especially the Ge data. However, the difference does not exceed 20% of the distorted-wave results, and in most cases the measurements agree with calculations within the experimental uncertainty.

In the following we will discuss the advantages and disadvantages of the two techniques for measuring ionization cross sections. The first method, which consists of the Ge-detector measurements, is the most fundamental approach. These measurements had the best statistics, no reflectivity correction, and were normalized to radiative-recombination cross sections, which are theoretically known to a high degree of accuracy. The disadvantages of the Ge-detector measurements involve the importance of resolution. For the elements we studied the Ge detector cannot distinguish between individual charge states in the $n=2$ radiative-recombination peak. We have attempted to fit the radiative-recombination peak; however, this procedure had a large uncertainty. Similarly, x rays from background ions cannot be resolved and can possibly contaminate the radiative-recombination peak. Furthermore, the Ge detector cannot resolve the heliumlike dielectronic-recombination x rays from those of the lithiumlike charge state. As a result, the Ge-detector measurements needed to be supplemented with data from the crystal spectrometer.

On the other hand, the advantages of the high-resolution data are (1) distinguishing between individual

TABLE III. Uncertainties (%) for the solid-state Ge-detector measurements. The fraction of I_{RR}^{tot} from lithiumlike ions was determined from crystal-spectrometer line ratios. All uncertainties were added in quadrature.

Source	Ti^{19+}	Cr^{21+}	Mn^{22+}	Fe^{23+}
Counting statistic	0.6	0.5	0.2	0.3
Unresolved background radiation	10.0	18.0	3.0	2.0
Be window and air transmission	9.5	6.0	4.0	3.2
Model adjustment of I_{RR}^{Li}	5.0	5.0	5.0	5.0
Fraction of I_{RR}^{tot} from lithiumlike ions	13.5	11.9	8.4	11.2
Total uncertainty	20.0	22.9	11.0	12.9

TABLE IV. Uncertainties (%) for the high-resolution von Hámos spectrometer measurements, normalized to theoretical [23] excitation cross sections for line q. All uncertainties were added in quadrature.

Source	Ti^{19+}	V^{20+}	Cr^{21+}	Mn^{22+}	Fe^{23+}
Counting statistics	3.8	2.3	2.5	1.4	3.7
Spectrometer response (W)	2.0	2.0	2.0	2.0	2.0
Radiative branching ratio	6.0	6.0	6.0	6.0	6.0
Model adjustment of I_q	5.0	5.0	5.0	5.0	5.0
Crystal response linearity	6.0	6.0	3.0	3.0	3.0
Total uncertainty	10.7	10.3	9.0	8.7	9.4

charge states in the $n=2\rightarrow 1$ direct excitation spectrum, which provides information on the charge-state balance and the measurement of the lithiumlike line q for normalization, and (2) providing information as to the amount of the lithiumlike dielectronic satellites present in each of the heliumlike dielectronic-recombination spectra. The main disadvantage of the high-resolution technique when compared to the Ge-detector method is that a further level of complexity is added. These measurements have less statistics, rely on calculated crystal reflectives and radiative branching ratios, and are normalized to excitation cross sections, which are not believed to be as well known as radiative recombination.

VI. CONCLUSION

We have measured the ionization cross sections of lithiumlike Ti, V, Cr, Mn, and Fe at the *KLL* resonance energy, i.e., at approximately 2.3 times the threshold energy for ionization. The measurements were made with an x-ray technique which has been discussed in detail. The x-ray data were compared to synthetic x-ray spectra calculated using an ionization-balance model with one free parameter. The x-ray data and the modeled spectra were in good agreement. This comparison gave important insight as to how the charge-state balance varied as the electron beam was alternated between the dielectronic-recombination resonances to values away from the resonances and was used to account for the contribution of charge-exchange recombination.

The ionization cross sections have been compared to the results from distorted-wave calculations using the codes of Zhang and Sampson [31]. The comparison shows excellent agreement overall.

In our high-resolution Bragg spectrometer measurement we determined the lithiumlike ionization cross sections by normalizing to theoretical excitation cross sections for the lithiumlike line q. This procedure can be reversed to infer the excitation cross sections of line q relative to theoretical ionization cross sections. Thus by reversing the normalization procedure our experimental approach represents a way of determining excitation cross sections, which is important as the excitation cross section of q is often more difficult to calculate than the lithiumlike ionization cross section.

ACKNOWLEDGMENTS

We wish to thank E. Magee and D. Nelson for their technical assistance in these measurements. This work was performed under the auspices of the U.S. Department of Energy by Lawrence Livermore National Laboratory under Contract No. W-7405-ENG-48.

[1] K. T. Dolder, M. F. A. Harrison, and P. C. Thonemann, Proc. R. Soc. London, Ser. A **264**, 367 (1961).
[2] D. C. Gregory, L. J. Wang, F. W. Meyer, and K. Rinn, Phys. Rev. A **35**, 3256 (1987).
[3] M. Sataka, S. Ohtani, D. Swenson, and D. C. Gregory, Phys. Rev. A **39**, 2397 (1989).
[4] D. C. Gregory, L. J. Wang, D. R. Swenson, M. Sataka, and S. J. Chantrenne, Phys. Rev. A **41**, 6512 (1990).
[5] A. Müller, G. Hofmann, K. Tinschert, and E. Salzborn, Phys. Rev. Lett. **61**, 1352 (1988).
[6] H.-J. Kunze, Space Sci. Rev. **13**, 565 (1972).
[7] C. Breton, C. DeMichelis, M. Finkenthal, and M. Mattioli, Phys. Rev. Lett. **41**, 110 (1978).
[8] R. U. Datla and J. R. Roberts, Phys. Rev. A **28**, 2201 (1983).
[9] J. S. Wang, H. R. Griem, R. Hess, W. L. Rowan, and T. P. Kochanski, Phys. Rev. A **33**, 4293 (1986).
[10] J. S. Wang, H. R. Griem, R. Hess, and W. L. Rowan, Phys. Rev. A **38**, 4761 (1988).
[11] M. A. Levin, R. E. Marrs, J. R. Henderson, D. A. Knapp, and M. B. Schneider, Phys Scr. **T22**, 157 (1988).
[12] R. E. Marrs, M. A. Levine, D. A. Knapp, and J. R. Henderson, Phys. Rev. Lett. **60**, 1715 (1988).
[13] P. Beiersdorfer, Nucl. Instrum. Methods B **56/57**, 1144 (1991).
[14] K. L. Wong, P. Beiersdorfer, D. Vogel, R. Marrs, and M. Levine, Z. Phys. D Suppl. **21**, S197 (1991).
[15] R. Ali, C. P. Bhalla, C. L. Cocke, and M. Stockli, Phys. Rev. Lett. **64**, 633 (1990).
[16] R. Ali, C. P. Bhalla, C. L. Cocke, M. Schulz, and M. Stockli, Phys. Rev. A **44**, 223 (1991).
[17] K. L. Wong, P. Beiersdorfer, R. E. Marrs, B. M. Penetrante, K. J. Reed, J. H. Scofield, D. A. Vogel, and R. Zasdzinski, Nucl. Instrum. Methods B **72**, 234 (1992).
[18] J. H. Scofield, Phys. Rev. A **40**, 3054 (1989).
[19] M. H. Chen, Phys. Rev. A **33**, 994 (1986).

[20] E. B. Saloman, J. H. Hubbell, and J. H. Scofield, At. Data Nucl. Data Tables **38**, 1 (1988).
[21] M. K. Inal and J. Dubau, J. Phys. B **22**, 3329 (1989).
[22] M. H. Chen, Phys. Rev. A **31**, 1449 (1985).
[23] H. L. Zhang, D. H. Sampson, and R. E. H. Clark, Phys. Rev. A **41**, 198 (1990).
[24] K. L. Wong, P. Beiersdorfer, R. E. Marrs, K. J. Reed, and D. A. Vogel, in *VIth International Conference on the Physics of Highly Charged Ions, Manhattan, KS, 1992,* edited by Patrick Richard, Martin Stöckli, C. Lewis Cocke, and C. D. Lin, AIP Conf. Proc. No. 274 (AIP, New York, 1993).
[25] I. G. Brown, J. E. Galvin, R. A. MacGill, and R. T. Wright, Appl. Phys. Lett. **49**, 1019 (1986).
[26] P. Beiersdorfer, R. E. Marrs, J. R. Henderson, D. A. Knapp, M. A. Levine, D. B. Platt, M. B. Schneider, D. A. Vogel, and K. L. Wong, Rev. Sci. Instrum. **61**, 2338 (1990).
[27] L. A. Vainshtein and U. I. Safronova, Phys. Scr. **31**, 519 (1985).
[28] W. Lotz, Z. Phys. **216**, 241 (1968).
[29] Y. S. Kim and R. H. Pratt, Phys. Rev. A **27**, 2913 (1983).
[30] R. K. Janev, D. S. Belić, and B. H. Bransden, Phys. Rev. A **28**, 1293 (1983).
[31] H. L. Zhang and D. H. Sampson, Phys. Rev. A **42**, 5378 (1990).